J. Fluid Mech. (2024), *vol*. 995, A2, doi:10.1017/jfm.2024.626

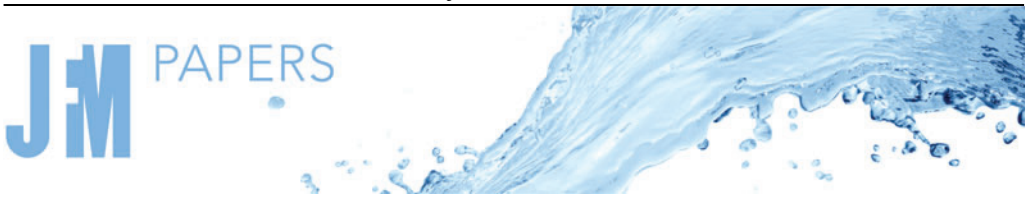

Self-similarity and recurrence in stability spectra of near-extreme Stokes waves

B. Deconinck[1], **S.A. Dyachenko**[2] **and A. Semenova**[1],†

[1]Department of Applied Mathematics, University of Washington, Seattle, WA 98195-3925, USA

[2]Department of Mathematics, State University of New York at Buffalo, Buffalo, NY 14260-2900, USA

(Received 23 April 2024; revised 15 July 2024; accepted 18 July 2024)

We consider steady surface waves in an infinitely deep two-dimensional ideal fluid with potential flow, focusing on high-amplitude waves near the steepest wave with a 120° corner at the crest. The stability of these solutions with respect to coperiodic and subharmonic perturbations is studied, using new matrix-free numerical methods. We provide evidence for a plethora of conjectures on the nature of the instabilities as the steepest wave is approached, especially with regards to the self-similar recurrence of the stability spectrum near the origin of the spectral plane.

Key words: waves/free-surface flows, surface gravity waves

1. Introduction

We consider the stability of spatially periodic waves that propagate with constant velocity without change of form, in potential flow of an ideal (incompressible and inviscid) two-dimensional fluid of infinite depth. The study of such wave profiles has been the subject of much previous work, going back to Stokes (1847) (also published in Stokes (1880*a*)). Stokes' work was followed by numerical computation of these waves by Michell (1893), and existence was proved in the works of Nekrasov (1921) and Levi-Civita (1925), see also Toland (1996) and Hur (2006) for existence of the global branch of wave profiles. The numerical study of these waves and the nature of their singularities was continued by Grant (1973), Schwartz (1974), Williams (1981), Williams (1985), Tanveer (1993), Cowley, Baker & Tanveer (1999), Baker & Xie (2011), Lushnikov (2016) and others.

In the context of water waves, such waves are usually referred to as Stokes waves. It was suggested by Stokes (1880*b*) that there exists a progressive wave of maximum height, and

† Email address for correspondence: asemenov@uw.edu

that the angle at the crest of this limiting wave should be $2\pi/3$. Rigorous proofs of these Stokes conjectures came much later. Toland (1978) showed global existence of the limiting Stokes wave, but did not prove that the angle at the crest is $2\pi/3$. This result was proved by Amick, Fraenkel & Toland (1982) and Plotnikov (1982) (reported in English in Plotnikov (2002)) independently. We refer to the Stokes wave of greatest height as the extreme wave and to waves of near-maximal amplitude as near-extreme waves. Even with the original Stokes conjectures resolved, the study of the graph of the wave profiles remains active, with a number of open problems, as detailed by Dyachenko, Hur & Silantyev (2023), see also below. The works by Longuet-Higgins & Fox (1977, 1978) and by Longuet-Higgins (2008) study the near-extreme waves using both asymptotic and numerical methods. The review by Haziot *et al.* (2022) discusses many currently active research directions.

The investigation of the stability of Stokes waves was begun in the works of Benjamin (1967), Benjamin & Feir (1967), Lighthill (1965) and Whitham (1967). Except for the influential experimental work by Benjamin & Feir (1967), the focus of these works was on the dynamics of small disturbances of small-amplitude periodic Stokes waves. They unveiled the presence of the modulational or Benjamin–Feir instability with respect to long-wave disturbances in water of sufficient depth, $kh > 1.363\ldots$; here h is the depth of the water and $k = 2\pi/L$, with L the period of the Stokes wave. The first rigorous results on the Benjamin–Feir instability were established by Bridges & Mielke (1995), followed up very recently by Nguyen & Strauss (2023) and Hur & Yang (2023). The numerical results of Deconinck & Oliveras (2011) reveal the presence of a figure-8 curve in the complex plane of the spectrum of the linear operator governing the linear evolution of the Stokes wave disturbances. Approximations to this figure-8 are obtained by Creedon & Deconinck (2023) and by Berti, Maspero & Ventura (2022), where the existence of the figure-8 was proven rigorously. Berti, Maspero & Ventura (2024) also examined the critical case $kh = 1.363\ldots$.

Deconinck & Oliveras (2011) also brought to the fore the presence of the so-called high-frequency instabilities, existing for narrow ranges of the disturbance quasiperiods. These instabilities were further studied by Creedon, Deconinck & Trichtchenko (2022) and by Hur & Yang (2023), where their existence was proven rigorously.

The instabilities mentioned above play a role in our study of the dynamics of large-amplitude Stokes waves, but we illustrate other instability mechanisms, not present for small-amplitude waves. Understandably, the study of large-amplitude Stokes waves, which cannot be thought of as perturbations of flat water, is harder, both from a computational and an analytical point of view. Nonetheless, some groundbreaking examinations have been done, for instance by Tanaka (1983), Longuet-Higgins & Tanaka (1997) and for near-extreme waves by Korotkevich *et al.* (2023). These authors all consider perturbations of the Stokes waves with respect to coperiodic (or superharmonic) disturbances, i.e. the Stokes waves and the disturbance have the same minimal period. Their results are recapped in detail below, as they are instrumental to our own investigations. The results in this manuscript follow those of Deconinck *et al.* (2023), as we present a computational study of the instabilities of periodic Stokes waves, under the influence of disturbances parallel to the propagation direction of the wave. It should be emphasized that all figures presented below are quantitatively correct unless they are described as 'schematic' in the caption. Similarly, all floating-point numbers given are approximate, of course, but all digits provided are believed to be correct.

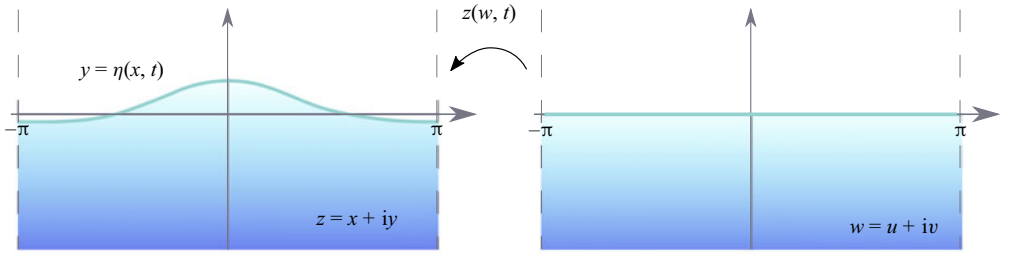

Figure 1. A schematic of the conformal map from the lower half-plane to the physical domain.

2. One-dimensional waves in water of infinite depth

The equations of motion governing the dynamics of the one-dimensional free surface of a two-dimensional irrotational, inviscid fluid (see figure 1*a*) are the Euler equations:

$$\Phi_{xx} + \Phi_{yy} = 0, \quad x \in \mathbb{R}, \quad y \in (-\infty, \eta(x,t)), \tag{2.1}$$

$$\eta_t = (-\Phi_x \eta_x + \Phi_y)|_{y=\eta(x,t)}, \quad x \in \mathbb{R}, \quad y = \eta(x,t), \tag{2.2}$$

$$\left(\Phi_t + \frac{1}{2}(\Phi_x^2 + \Phi_y^2)\right)\Big|_{y=\eta(x,t)} + g\eta = 0, \quad x \in \mathbb{R}, \quad y = \eta(x,t), \tag{2.3}$$

$$\lim_{y\to-\infty} \Phi_y = 0, \quad x \in \mathbb{R}. \tag{2.4}$$

Here $y = \eta(x,t)$ is the equation of the free surface and $\Phi(x,y,t)$ is the velocity potential (i.e. the velocity in the fluid is $v = (\Phi_x, \Phi_y)$), subscripts denote partial derivatives, x and y are the horizontal and vertical coordinate respectively, t denotes time and g is the acceleration due to gravity. We ignore the effects of surface tension. Although the Stokes waves are 2π-periodic, it is important to pose the problem above on $x \in \mathbb{R}$, since the perturbations we consider are not necessarily periodic. The first equation expresses the divergence-free property of the flow under the free surface determined by $\eta(x,t)$. The second and third equations are nonlinear boundary conditions determining the free surface: the kinematic condition (2.2) expresses that the free surface changes in the direction of the normal derivative to the surface (particles on the surface remain on the surface), whereas the dynamic condition (2.3) states the continuity of pressure across the surface. Atmospheric pressure has been equated to zero, without loss of generality.

Since the location of the surface $y = \eta(x,t)$ is the main focus of the water wave problem, different reformulations have been developed that eliminate the velocity potential in the bulk of the fluid as an unknown. Zakharov (1968) shows how the problem (2.1)–(2.4) can be recast in terms of only the surface variables $\eta(x,t)$ and $\varphi(x,t) = \Phi(x,\eta(x,t),t)$, and the dynamics of $\eta(x,t)$ and $\varphi(x,t)$ is governed by an infinite-dimensional Hamiltonian system with $\eta(x,t)$ and $\varphi(x,t)$ as canonical variables. The Hamiltonian is the total energy of the system (with potential energy renormalized to account for infinite depth), which depends on the velocity potential $\Phi(x,y,t)$ in the bulk of the fluid.

To avoid the dependence on the bulk, Zakharov's formulation uses the Dirichlet-to-Neumann operator (DNO), producing the normal derivative of the velocity potential at the free surface (the right-hand side of (2.2)) from the values of $\varphi(x,t)$. For small-amplitude waves, the DNO is conveniently expressed as a series, as done by Craig & Sulem (1993). For large-amplitude waves, such an expansion is not readily available, and the DNO has to be approximated numerically. To avoid doing so, we use conformal variables, see figure 1:

for a 2π-periodic wave, a time-dependent conformal transformation maps the half-plane in the $w = u + \mathrm{i}v$ plane ($(u, v) \in [-\pi, \pi] \times (-\infty, 0]$) into the area $(x, y) \in [-\pi, \pi] \times (-\infty, \eta]$ in the physical $z = x + \mathrm{i}y$ plane occupied by the fluid. The horizontal line $v = 0$ is mapped into the fluid surface $y = \eta(x, t)$. The implicit equations of motion in conformal variables are constructed in the works of Ovsyannikov (1973), see also Tanveer (1991), Zakharov, Kuznetsov & Dyachenko (1996) and Dyachenko (2001). We use this implicit formulation to study the stability of Stokes waves.

From these works, the conformal map $z(w, t) = x(w, t) + \mathrm{i}y(w, t)$ is a complex-analytic function in $\mathbb{C}^-$ that approaches the identity map $z(w, t) \to w$ as $w \to -i\infty$, the image of a point at infinite depth. In the conformal variables, the Hamiltonian has the form

$$\mathcal{H} = \frac{1}{2}\int_{-\pi}^{\pi} \psi \hat{k}\psi \,\mathrm{d}u + \frac{g}{2}\int_{-\pi}^{\pi} y^2 x_u \,\mathrm{d}u, \tag{2.5}$$

where $\psi(u, t) = \varphi(x, t)$ and the operator $\hat{k} = -\hat{H}\partial_u$. Here $\hat{H}$ is the periodic Hilbert transform defined by the principal-value integral

$$\hat{H}f(u) = \frac{1}{2\pi}\fint_{-\pi}^{\pi} f(u') \cot\frac{u' - u}{2}\mathrm{d}u'. \tag{2.6}$$

Equivalently, the Hilbert transform can be defined by its action on Fourier harmonics, $\hat{H}\,\mathrm{e}^{\mathrm{i}ku} = \mathrm{i}\,\mathrm{sign}(k)\,\mathrm{e}^{\mathrm{i}ku}$. The equations of motion are derived by taking variational derivatives of the action $\mathcal{S} = \int \mathcal{L}\,\mathrm{d}t$ with respect to x, y and ψ. The Lagrangian has the form

$$\mathcal{L} = \int_{-\pi}^{\pi} \psi\,(y_t x_u - y_u x_t)\,\mathrm{d}u - \mathcal{H} + \int_{-\pi}^{\pi} f(u)(y - \hat{H}[x - u])\,\mathrm{d}u, \tag{2.7}$$

where the Lagrange multiplier $f(u)$ is chosen to enforce the relation $x(u, t) = u - \hat{H}[y(u, t)]$. We refer to the work of Dyachenko *et al.* (1996) for the complete derivation of the equations of motion in conformal variables:

$$y_t x_u - y_u x_t = -\hat{H}\psi_u, \tag{2.8}$$

$$x_t\psi_u - x_u\psi_t - \hat{H}[y_t\psi_u - y_u\psi_t] = g\left(x_u y - \tfrac{1}{2}\hat{H}\partial_u y^2\right). \tag{2.9}$$

2.1. *Travelling waves*

Using the conformal variables formulation (2.8)–(2.9), the Stokes waves are obtained by looking for a solution $y = y(u - ct)$, $\psi = \psi(u - ct)$, corresponding to stationary solutions in a frame of reference moving with constant speed c in physical variables, see Dyachenko, Lushnikov & Korotkevich (2014). This gives rise to the so-called Babenko (1987) equation:

$$(c^2\hat{k} - g)y - \frac{g}{2}(\hat{k}y^2 + 2y\hat{k}y) = 0. \tag{2.10}$$

Since we are interested in the stability of near-extreme Stokes waves, the accurate numerical solution of (2.10) for near-limiting values of the speed is required. Details of such computations for the Babenko equation (2.10) are given by Dyachenko, Lushnikov & Korotkevich (2016). In what follows, the ratio of the crest-to-trough height H to wavelength L is used as the definition of wave steepness $s = H/L$. The limiting Stokes wave has the steepness $s_{lim} = 0.1410634839\ldots$ and speed $c_{lim} = 1.0922850485\ldots$ as computed by Dyachenko *et al.* (2023).

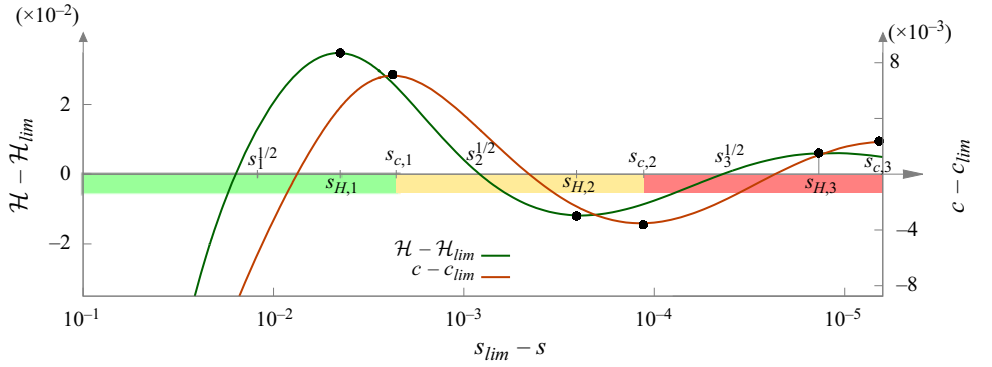

Figure 2. A schematic of the oscillations of the Hamiltonian $\mathcal{H}$ (green) and the velocity c (red) relative to their limit values as steepness s increases to its limiting 120° Stokes wave value, using a logarithmic scale for the steepness s relative to its limit value s_{lim}. In the green region, the waves are unstable with respect to the first Benjamin–Feir branch and the first localized instability branch, see § 3. In the yellow region, they are unstable with respect to the second branches, and so on. The steepnesses $s_{c,n}$ and $s_{H,n}$ correspond to the steepness values where the velocity c and the Hamiltonian $\mathcal{H}$ have extreme values.

It is known that the speed c and the Hamiltonian $\mathcal{H}$ oscillate as a function of the wave steepness s, for values near the limiting value s_{lim}, see Longuet-Higgins & Fox (1978). It is believed there is an infinite number of such oscillations. They are presented schematically in figure 2. The other details of this figure constitute some of the main results of this paper, discussed below.

2.2. *Linearization about a Stokes wave*

In a reference frame travelling with the velocity of a Stokes wave, the Babenko equation describes a stationary solution of (2.8)–(2.9). The linear stability of these Stokes waves is determined by the eigenvalue spectrum of the linearization in this travelling frame. To obtain the linearization, we transform (2.8)–(2.9) to a moving frame, using

$$y(u,t) \to y(u-ct,t), \quad \text{and} \quad x(u,t) \to u - \hat{H}y(u-ct,t), \tag{2.11a,b}$$

$$\psi(u,t) \to \phi(u-ct,t) - c\hat{H}y(u-ct,t), \tag{2.12}$$

as in Dyachenko & Semenova (2023*a*). The nonlinear system (2.8)–(2.9) in the moving frame becomes

$$x_u y_t - y_u x_t = -\hat{H}(\phi_u - c), \tag{2.13}$$

$$x_u\phi_t - x_t\phi_u - \hat{H}[y_u\phi_t - y_t\phi_u] + 2cx_t = c^2\hat{k}y - g(x_u y - \hat{H}[yy_u]). \tag{2.14}$$

The linearization about a Stokes wave is found by substituting

$$y(u,t) \to y(u) + \delta y(u,t) + \cdots \quad \text{and} \quad \phi(u,t) \to 0 + \delta\phi(u,t) + \cdots. \tag{2.15a,b}$$

Here $y(u)$ corresponds to the Stokes wave and $\delta y(u,t)$, $\delta\phi(u,t)$ are small perturbations. Retaining only linear terms in δy and $\delta\phi$ leads to the following evolution equations for the

perturbations δy and $\delta\phi$:

$$\hat{\Omega}_{21}^{\dagger}\delta\phi_t - 2c\hat{H}\delta y_t = \hat{S}_1\delta y, \tag{2.16}$$

$$\hat{\Omega}_{21}\delta y_t = \hat{k}\delta\phi, \tag{2.17}$$

where the operator $\hat{\Omega}_{21}$ is defined via $\hat{\Omega}_{21}f = x_u f + y_u\hat{H}f$. The operator $\hat{\Omega}_{21}^{\dagger}$ is its adjoint: $\hat{\Omega}_{21}^{\dagger}f = x_u f - \hat{H}[y_u f]$ and

$$\hat{S}_1(y)\delta y = (c^2\hat{k} - g)\delta y - g[y\hat{k}\delta y + \delta y\hat{k}y + \hat{k}(y\delta y)]. \tag{2.18}$$

This is rewritten in matrix form as

$$\hat{\boldsymbol{L}}\partial_t\begin{bmatrix}\delta\phi\\ \delta y\end{bmatrix} = \hat{\boldsymbol{M}}\begin{bmatrix}\delta\phi\\ \delta y\end{bmatrix}, \tag{2.19}$$

with

$$\hat{\boldsymbol{L}} = \begin{bmatrix}0 & \hat{\Omega}_{21}\\ \hat{\Omega}_{21}^{\dagger} & -2c\hat{H}\end{bmatrix}, \quad \hat{\boldsymbol{M}} = \begin{bmatrix}\hat{k} & 0\\ 0 & \hat{S}_1\end{bmatrix}. \tag{2.20a,b}$$

We examine the effect of quasiperiodic perturbations δy, $\delta\phi$ using the Fourier–Floquet–Hill approach described in Deconinck & Kutz (2006) and Deconinck & Oliveras (2011). The time dependence for δy and $\delta\phi$ is found using separation of variables. Moreover, in order to consider quasiperiodic perturbations we use a Floquet-Bloch decomposition in space,

$$\begin{bmatrix}\delta y(u,t)\\ \delta\phi(u,t)\end{bmatrix} = \mathrm{e}^{(\mathrm{i}\lambda t + \mathrm{i}\mu u)}\begin{bmatrix}\delta y(u)\\ \delta\phi(u)\end{bmatrix}, \tag{2.21}$$

where $\mu \in (-1/2, 1/2]$ is the Floquet parameter and $\lambda(\mu) \in \mathbb{C}$ is the eigenvalue. The resulting μ-dependent spectral problem is solved using a Krylov-based method and the shift-and-invert technique, see Dyachenko & Semenova (2023*b*). Details on Krylov methods are presented by Stewart (2002). We refer to the spectrum obtained this way as the stability spectrum of the Stokes wave. Note that the Floquet parameter is defined modulo 1, thus $\mu = 1/2$ is equivalent to $\mu = -1/2$, see Deconinck & Kutz (2006).

3. Instability

3.1. *The oscillating velocity and Hamiltonian*

Both the velocity c and the Hamiltonian $\mathcal{H}$ depend on the Stokes wave. As the steepness s of the Stokes wave increases and approaches its limiting value s_{lim}, both quantities are not monotonic, as observed by Longuet-Higgins (1975). In fact, Longuet-Higgins & Fox (1977, 1978) produce an asymptotic result that implies the presence of an infinite number of oscillations for both quantities. These oscillations were studied more by Maklakov (2002), Dyachenko *et al.* (2016) and Lushnikov, Dyachenko & Silantyev (2017), and very recently by Silantyev (2019). To our knowledge, no proof of an infinite number of oscillations in velocity c and Hamiltonian $\mathcal{H}$ exists.

We denote the steepness of a wave at the nth turning point of the speed by $s_{c,n}$, $n = 0, 1, 2, \ldots$, with $s_{c,0} = 0$. Similarly, the nth extremizer of the Hamiltonian is denoted by $s_{H,n}$. These critical values of the velocity and the Hamiltonian are important for changes in the stability spectrum, as shown below. For the Hamiltonian, the importance of these values is known, due to the works of Tanaka (1983, 1985), Saffman (1985) and

Longuet-Higgins & Tanaka (1997), for instance. It appears that these extremizing values interlace, so that $s_{c,n} < s_{H,n+1} < s_{c,n+1}$, $n = 0, 1, \ldots$.

In the recent work of Dyachenko & Semenova (2023*b*), a conjecture is made about an infinite number of secondary bifurcations associated with the Floquet multiplier $\mu = 1/2$, corresponding to perturbations whose period is twice that of the Stokes wave. It is unclear how these bifurcations are related to those in the works of Chen & Saffman (1980), Longuet-Higgins (1985) and Zufiria (1987), since those works do not introduce a Floquet parameter. However, their importance to the stability results presented here is demonstrated below. We denote the steepness associated with the nth secondary bifurcation point by $s_n^{1/2}$, $n = 1, 2, \ldots$. Further, we observe that $s_{c,n} < s_n^{1/2} < s_{H,n}$. These values are included in the schematic of figure 2.

It is convenient to break up the range of steepness s from $s = 0$ to $s = s_{lim}$ in intervals from one extremizer of the wave speed to the next. For example, the first interval starts at the primary bifurcation $s = 0$ and ends at the first maximizer of the wave speed $s = s_{c,1}$; the second interval starts at $s = s_{c,1}$ and ends at the first minimizer of the wave speed $s_{c,2}$, and so on. The length of each interval shrinks as the extreme wave is approached, and following Longuet-Higgins & Fox (1978), we use a logarithmic scaling as illustrated in figure 2. Note that, because of the observed interlacing of the extremizers of the wave speed, those of the Hamiltonian, and the secondary bifurcations, each interval contains one extremizer of the Hamiltonian and one secondary bifurcation point.

3.2. *A cycle of changes in the spectrum*

As the steepness increases and each interval is traversed, an instability emerges from $\lambda = 0$ in the spectral plane, giving rise to a sequence of $\lambda(\mu)$-curves with changing topology, see figure 3. These changes for $s \in [s_{c,0} = 0, s_{c,1})$ are described below.

(i) Initially, at $s_{c,0}$, a figure-8 emerges from the origin, expanding in size as steepness increases (figure 3*a*,*b*).

(ii) At an isolated value of the steepness $s = s_{h,1}$, both tangents of the figure-8 at the origin become vertical, resulting in an hourglass shape (figure 3*c*).

(iii) Next, the lobes of the figure-8 detach from the origin, forming two disjoint isles qualitatively reminiscent of the high-frequency instabilities of Deconinck & Oliveras (2011). The band of Floquet values parameterizing the isles shrinks away from $\mu = 0$ as the steepness increases (figure 3*d–h*).

(iv) At $s = s_1^{1/2}$, eigenvalues with Floquet parameter $\mu = 1/2$ bifurcate away from the origin onto the real line, creating an oval of eigenvalues with centre at the origin, parameterized by Floquet values centred about $\mu = 1/2$, see figure 3(*f–h*).

(v) As the steepness increases, the oval around the origin deforms to a bean shape, eventually reabsorbing the remnants of the figure-8 (figure 3*j*). More detail on the changes in these remnants and their reabsorption is presented in figures 5 and 8.

(vi) At $s = s_{H,1}$, the bean shape pinches to form a figure-∞. The double point of the figure-∞ is at the origin and has a Floquet parameter $\mu = 0$. Thus, it corresponds to perturbations with the same period as the Stokes wave, see Korotkevich *et al.* (2023) and Dyachenko & Semenova (2023*a*). In figure 3(*k*) this coperiodic (or superharmonic) eigenvalue is marked in green. The unstable eigenvalue with $\mu = 1/2$ is marked in red and gives rise to the most unstable mode for the wave with steepness $s = s_{H,1}$.

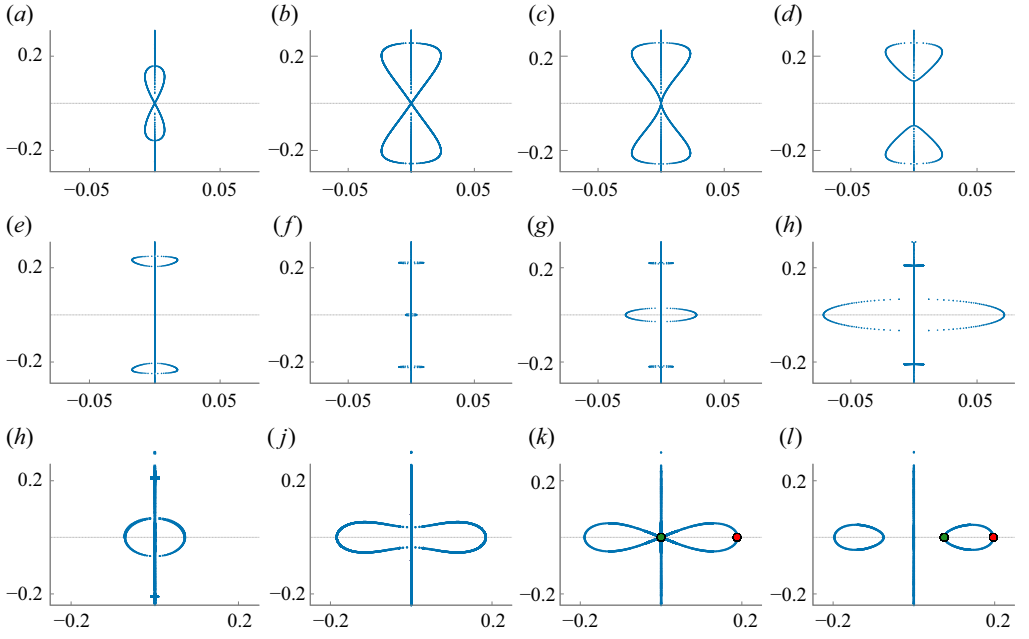

Figure 3. Spectra in the vicinity of the origin for increasing steepness s. A detailed description is found in the main text. Here (*a*) $s = 0.0449032652$, (*b*) $s = 0.1042102092$, (*c*) $s = 0.1090618215$, (*d*) $s = 0.1122542820$, (*e*) $s = 0.1214481620$, (*f*) $s = 0.1289100582$, (*g*) $s = 0.1292029131$, (*h*) $s = 0.1307253066$, (*j*) $s = 0.1364173038$, (*k*) $s = 0.1366036552$, (*l*) $s = 0.1368557681$. Note that (*h*) is repeated, with changing scales.

(vii) As s increases beyond $s_{H,1}$, the figure-∞ splits off from the origin into a pair of symmetric lobes, one moving to the right, the other to the left (figure 3*l*). Further interesting changes in the shape of these lobes are observed as the steepness increases and they move away from the origin, see Deconinck *et al.* (2023) and figure 4. Importantly, we observe that the most unstable mode for this range of steepness s is either coperiodic with the Stokes wave ($\mu = 0$, green dot in figure 4) or has twice its period, i.e. it is subharmonic with $\mu = 1/2$ (red dot in figure 4). Figure 4 illustrates two interchanges between these modes. We conjecture that such interchanges recur an infinite number of times as $s \to s_{lim}$. Note that the difference between $s_{lim} = 0.1410634839$ and the steepness in the final panel of figure 4 is approximately 0.000425 or 0.3 %.

Below we focus on what happens near the origin of the spectral plane as the steepness continues to increase, ever getting closer to its extreme value.

3.3. *The Benjamin–Feir instability*

We observe that a figure-8 shape in the stability spectrum emerges from the origin when the steepness $s = s_{c,n}$, an extremizer of the velocity. The first three extrema of the velocity appear at the following values:

$$s_{c,0} = 0, \tag{3.1}$$

$$s_{c,1} = 0.138753, \tag{3.2}$$

$$s_{c,2} = 0.140920. \tag{3.3}$$

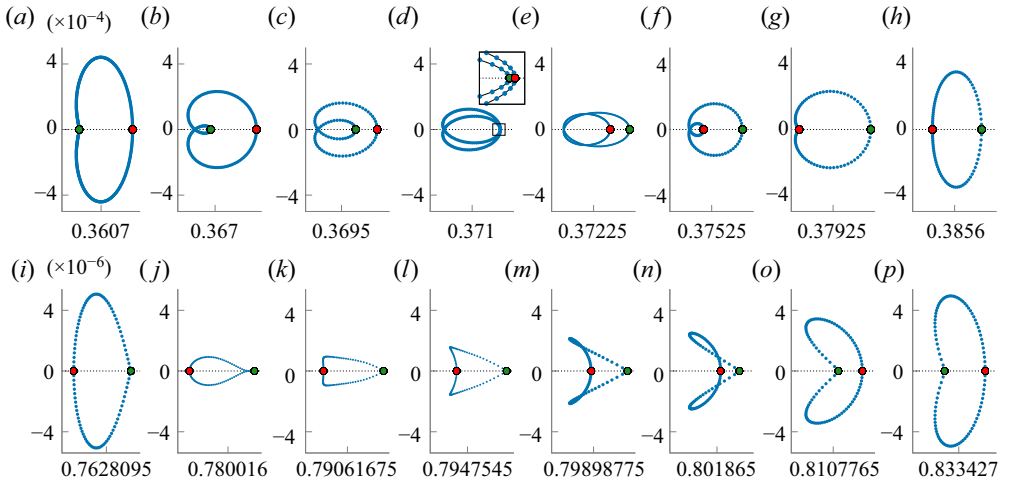

Figure 4. As steepness increases, the symmetric lobes of the figure-∞ in figure 3(k) detach and move away from the origin while shrinking in size. Here we track the spectrum of the lobe with highest real part, for increasing steepness (a) $s = 0.1394245282$, (b) $s = 0.1394647831$, (c) $s = 0.1394802926$, (d) $s = 0.1394894509$, (e) $s = 0.1394970022$, (f) $s = 0.1395148411$, (g) $s = 0.1395380437$, (h) $s = 0.1395744737$, (i) $s = 0.1405658442$, (j) $s = 0.1405850778$, (k) $s = 0.1405964046$, (l) $s = 0.1406007221$, (m) $s = 0.1406050801$, (n) $s = 0.1406080087$, (o) $s = 0.1406169126$, (p) $s = 0.1406384552$. Eigenvalues corresponding to the Floquet exponents $\mu = 0$ and $\mu = 0.5$ are marked by green and red circles, respectively. A detailed description is found in the main text.

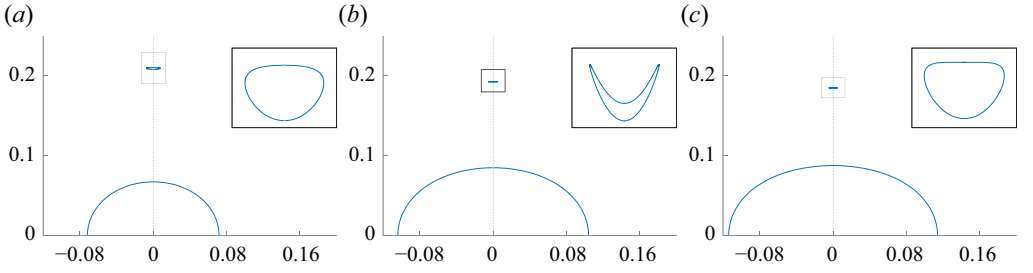

Figure 5. Changes in the Benjamin–Feir remnant as it approaches the oval at the origin, with steepness (a) $s = 0.1307253066$, (b) $s = 0.1323979204$ and (c) $s = 0.1329490573$.

For small-amplitude waves (i.e. waves with steepness s near $s_{c,0} = 0$), the figure-8 corresponds to the well-studied classical Benjamin–Feir, or the modulational instability. In what follows we refer to instabilities manifested through a figure-8 in the spectral plane as Benjamin–Feir instabilities.

We refer to the Benjamin–Feir instability branches starting at steepness $s_{c,n}$ as the $(n+1)$th Benjamin–Feir branch, denoted BFI, BFII, BFIII and so on. Below, we show that eigenvalues on the figure-8 near the origin (for BFII and BFII) give rise to modulational instabilities, as they do for small-amplitude waves, see Benjamin (1967) and Whitham (1967).

All the Benjamin–Feir branches that we compute experience the sequence of changes for increasing steepness described above: they grow in size, their tangents at the origin become vertical followed by pinching off of the figure-8, resulting in the formation of isole on the positive and negative imaginary axis. For each branch BFI, BFII and BFIII, we determine

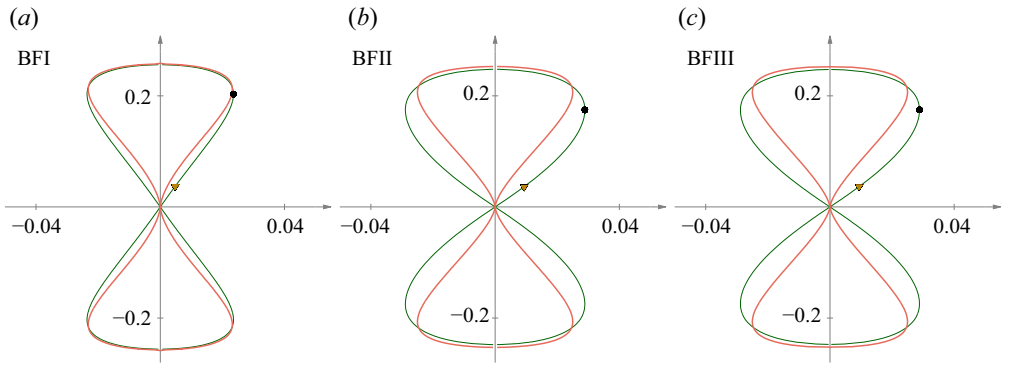

Figure 6. The figure-8 component of the eigenvalue spectrum, showing the Benjamin–Feir instability branches BFI, BFII and BFIII for Stokes waves of steepness (*a*) $s = 0.1045109822$ (green) and $s = 0.1092129256$ (red); (*b*) $s = 0.1398401087$ (green) and $s = 0.1401021466$ (red); (*c*) $s = 0.1409908317$ (green) and $s = 0.1410079370$ (red). The green curves are associated with the maximal instability growth on the corresponding Benjamin–Feir branch, with the black points marking the eigenvalues with largest real part, given in table 1. The red hourglass curves correspond to the steepness when the figure-8 tangents at the origin become vertical, leading to the figure-8 detaching from the origin in the spectral plane. The points marked by gold triangles close to the origin have Floquet exponent $\mu = 1/10$.

	s	λ	μ
BFI	0.1045109822	$0.0235702 + 0.2029603\mathrm{i}$	0.46376
BFII	0.1398401087	$0.0288896 + 0.1746076\mathrm{i}$	0.45743
BFIII	0.1409908317	$0.0288299 + 0.1747554\mathrm{i}$	0.45774

Table 1. The Benjamin–Feir instability parameters for the figure-8 with the largest growth rate, first three branches.

the figure-8 that gives rise to the eigenvalue with the largest real part, i.e. the maximal growth rate, see figure 6. Table 1 displays these values of steepness, the corresponding eigenvalue with maximal real part and its Floquet exponent, for BFI, BFII and BFIII. These computations illustrate that the widest figure-8 (green curves in figure 6) settles down to a universal shape as the extreme wave is approached, since figure 6*b* and figure 6*c* appear indistinguishable). The values in table 1 confirm this visual inspection. Further, for BFI, BFII and BFIII, we compute the hourglass shapes resulting from the figure-8s with vertical tangents at the origin, see figure 6. We overlay these shapes in figure 7, plotting the real part of the spectrum as a function of the Floquet parameter. This figure illustrates convergence to a universal hourglass shape as the steepest wave is approached. We conjecture that an infinite number of Benjamin–Feir instability branches exist as the steepest wave is approached and that all of them experience a universal sequence of transitions.

Finally, using the points marked by triangles in figure 6, we examine the eigenfunctions of (2.19). The eigenfunctions related to BFI, BFII and BFIII are visibly different, while their spectra in figures 6 and 7 are, to the eye, indistinguishable. A second observation is that these eigenfunctions are indeed modulational in nature: figure 7 displays 10 ($= 1/\mu$) Stokes wave periods of the eigenfunctions. Although their effect is increasingly localized at the crest in each wave period, there is a more global modulational effect when many periods are considered. Thus, even the BFII and BFIII instabilities, for μ close to zero, deserve the modulational instability moniker.

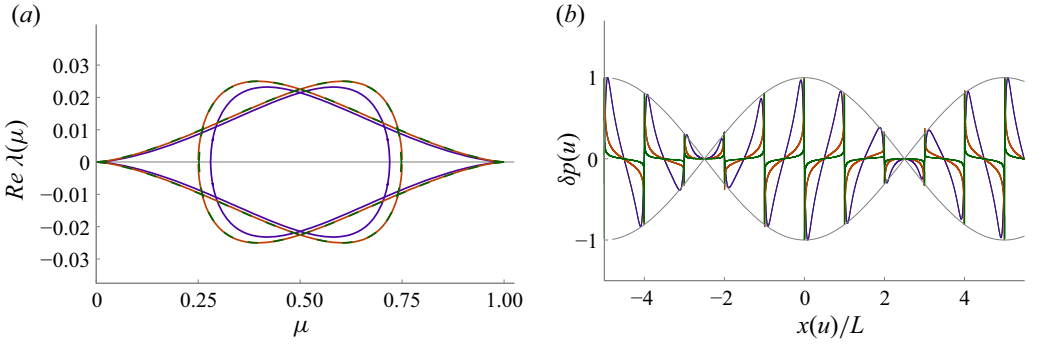

Figure 7. (*a*) The growth rate Re λ as a function of the Floquet exponent μ for BFI, BFII and BFIII are shown in purple, dashed green and dashed red, respectively. The curves are associated with hourglass cases of the BFI, BFII and BFIII figure-8s, the red curves in figure 6. (*b*) The unstable eigenfunctions associated with the triangular marker in figure 6(*a–c*) are coloured purple, red and green, respectively. The envelope for all three is well described by $\cos(\mu x/L)$ with $\mu = 1/10$ and $L = 2\pi$. Strong localization of the peaks of the eigenfunctions at the wave crests of the Stokes waves is observed as the wave steepness increases.

3.4. *The localized instability*

The nth oval emerges from the origin of the spectral plane as the steepness increases past $s_n^{1/2}$. We observe that $s_n^{1/2} > s_{h,n}$, the value of the steepness for which the nth Benjamin–Feir figure-8 separates from the origin. Thus, prior (i.e. for $s < s_n^{1/2}$) to these ovals emerging from the origin, the spectrum near the origin is confined to the imaginary axis. The primary, secondary and tertiary ovals form at the steepnesses

$$s_1^{1/2} = 0.128903, \tag{3.4}$$

$$s_2^{1/2} = 0.140487, \tag{3.5}$$

$$s_3^{1/2} = 0.141032049, \tag{3.6}$$

which correspond to steepnesses at which 4π-periodic Stokes waves bifurcate from the primary, 2π-periodic wave branch, see Dyachenko & Semenova (2023*b*).

The changing topology of the primary oval for $s > s_1^{1/2}$ is shown in figures 3 and 4. More detail is presented in figure 8. The oval develops for $s_1^{1/2} \leq s < s_{H,1}$. The oval stage is followed by a symmetric bean shape with a narrowing neck as steepness approaches $s_{H,1}$. The maximal growth rate associated with the localized instability quickly overtakes the maximal growth rate associated with the Benjamin–Feir isola higher on the imaginary axis, see Deconinck *et al.* (2023). Shortly before the steepness s reaches $s_{H,1}$, the first extremizer of the Hamiltonian, the remnant of the Benjamin–Feir instability isola merges with the localized instability branch bean, as shown in figure 8(*b*).

We observe the recurrence of the process described above two more times, for the secondary and tertiary ovals that form at $s = s_2^{1/2}$ and $s = s_3^{1/2}$, respectively. This leads to the conjecture of an infinite number of such recurrences, the nth one born at $s = s_n^{1/2}$, leading to the formation of the oval, gradually deforming to a bean shape, which pinches off at $s = s_{H,n}$, after which the resulting lobes move away from the origin along the real axis, ever decreasing in diameter. For $s > s_{H,n}$, the lobes are parameterized by the full range of Floquet exponents $\mu \in [-1/2, 1/2)$. Further, for $s \in (s_{H,n}, s_{c,n+1})$ there is no component of the spectrum other than the imaginary axis.

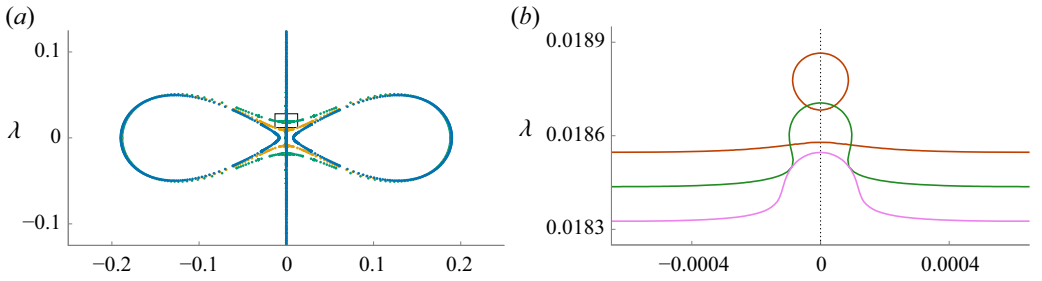

Figure 8. (*a*) Bean-shaped stage of the localized instability for $s = 0.1365552495 < s_{H,1}$ (green), $s = 0.1365917123 < s_{H,1}$ (gold) and $s = 0.1366066477 > s_{H,1}$ (blue). (*b*) Zoom-in on the remnant of the primary Benjamin–Feir isole as it is absorbed into the first localized branch at $s = 0.1365546598$ (red), $s = 0.1365552495$ (green) and $s = 0.1365558392$ (pink).

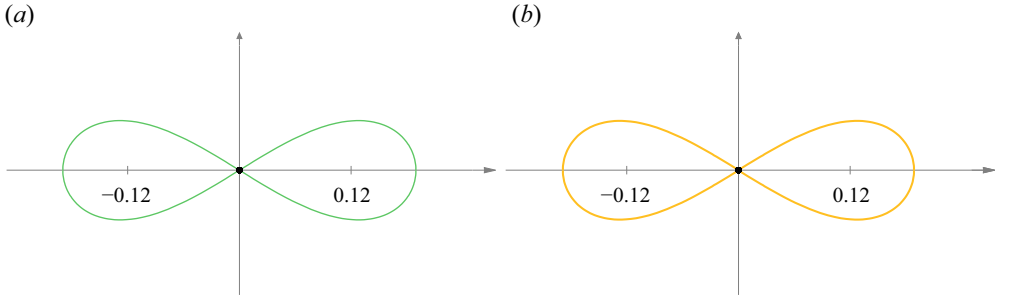

Figure 9. (*a*) The figure-∞ component of the instability spectrum appears at the first extremum of the Hamiltonian at $s_{H,1} = 0.1366035$. (*b*) The second figure-∞ component of the instability spectrum occurs for the wave with steepness $s_{H,2} = 0.1407965$ at the second extremum of the Hamiltonian. The difference between the real and imaginary parts of the two curves as a function of the Floquet exponent μ is less than 10^{-3}.

The first two figure-∞s are shown in figure 9. Like the figure-8s, they settle down to a universal shape as $s \to s_{lim}$. The difference between the real and imaginary parts of these first two figure-∞s as a function of the Floquet exponent never exceeds 10^{-3}.

Some eigenfunctions associated with the figure-∞ are displayed in figures 10 and 11. For Floquet exponents close to zero (green and gold graphs), the modulational effect of the perturbation is clear from the polar plots. For other Floquet exponents (e.g. red and blue), the perturbation does not have a distinct modulational character. As for other high-amplitude Stokes waves, the localization of the eigenfunction (and thus the perturbation) near the crest of the waves is increasingly pronounced as $s \to s_{lim}$.

When the oval forms at $s = s_n^{1/2}$, its eigenvalue with largest real part is real and has Floquet exponent $\mu = 1/2$, leading to eigenfunctions that have double the period of the Stokes wave. After pinch off, $s > s_{H,n}$, the left-most eigenvalue of the right lobe has $\mu = 0$ (coperiodic eigenfunctions). As for the primary lobe, we conjecture that the most unstable mode on the right lobe is either the $\mu = 0$ or the $\mu = 1/2$ mode, which interchange an infinite number of times as $s \to s_{lim}$, see Deconinck *et al.* (2023). As remarked above, the profile of the eigenfunction is strongly localized at the crests of the Stokes wave. Modes with μ close to 0 have an envelope containing roughly $1/\mu$ periods of the Stokes wave and could be called modulational. However, in contrast to the Benjamin–Feir instabilities, for these instabilities the $\mu = 0$ mode itself is unstable. For this reason, we refer to the instabilities emerging from the figure-∞s as localized instabilities.

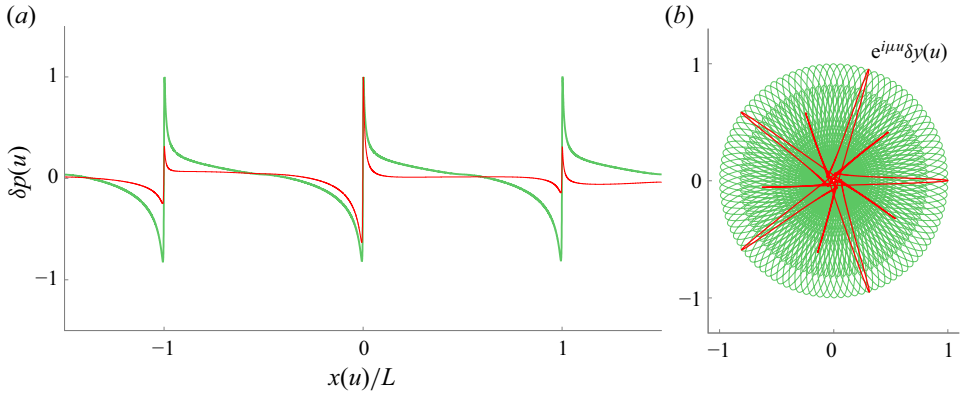

Figure 10. (*a*) For the wave with $s_{H,1} = 0.1366035$ in figure 9(*a*), the perturbation associated with $\mu = 0.01$ (green), with the eigenvalue $\lambda = 0.06106383 + 0.03263364\mathrm{i}$ and its complex conjugate $\bar{\lambda}$. The perturbation is given by $\delta p = Re[e^{i\mu u}\delta y]$. The red curve shows the same for $\mu = 0.2$, with eigenvalue $\lambda = 0.1600750 + 0.04326491\mathrm{i}$ and its complex conjugate $\bar{\lambda}$. Only the interval $-3\pi < x < 3\pi$ is shown from the $2\pi/\mu$-periodic function. (*b*) Polar plot, $e^{i\mu u}\delta y(u)$, where real and imaginary parts are plotted along the horizontal and vertical axes, respectively.

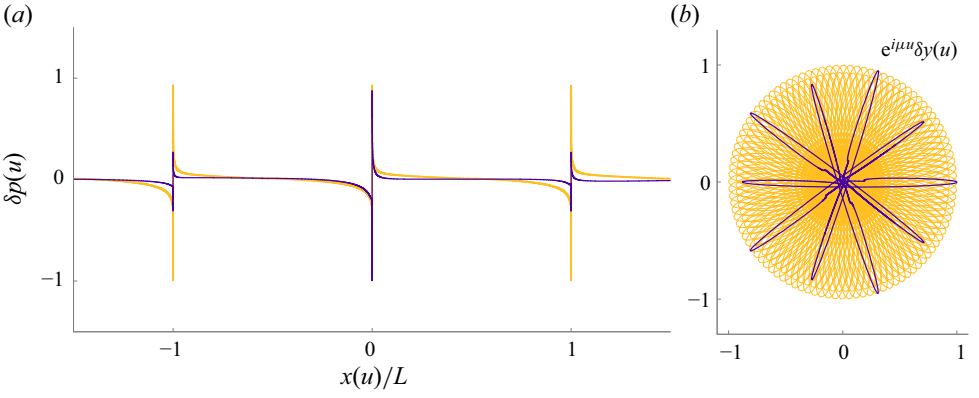

Figure 11. (*a*) For the wave with $s_{H,2} = 0.1407965$ in figure 9(*b*), the perturbation associated with $\mu = 0.01$ (gold) with the eigenvalue $\lambda = 0.06075090 + 0.03248890\mathrm{i}$, and its complex conjugate $\bar{\lambda}$. The perturbation is given by $\delta p = Re[e^{i\mu u}\delta y]$. The purple curve shows the same for $\mu = 0.2$. Only the interval $-3\pi < x < 3\pi$ is shown from the $2\pi/\mu$-periodic function. (*b*) Polar plot, $e^{i\mu u}\delta y(u)$, where real and imaginary parts are plotted along the horizontal and vertical axes, respectively.

3.5. *The maximal growth rate*

We track the maximum growth rate γ (i.e. we track the eigenvalues with the largest real part) of the Benjamin–Feir and localized instabilities (plotted in black dotted and solid lines) as a function of the steepness of the Stokes wave in figure 12. The maximum growth rate for BFI, BFII and BFII are presented by green, blue and purple curves, respectively. Steepnesses at which the dominant instability switches from the Benjamin–Feir to the corresponding localized branch are marked by circles. These switches are presented in the corresponding insets. The steepness values where the maximal growth rates for BFI and BFII vanish, correspond to the case where the Benjamin–Feir remnants are absorbed into the localized instabilities.

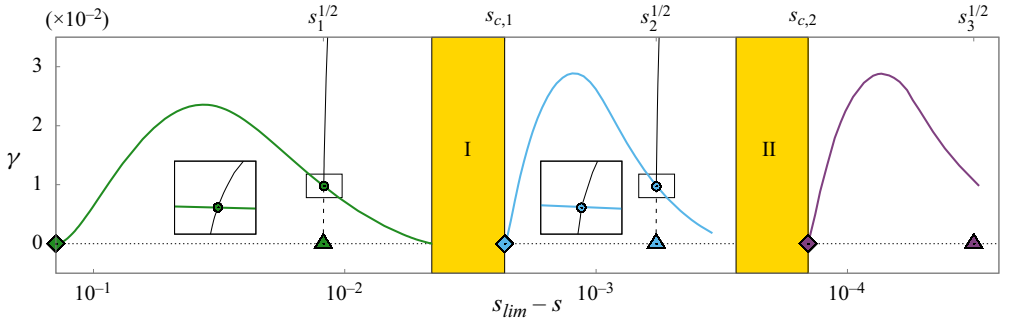

Figure 12. The primary BF instability emerges at steepness $s = 0$ for small-amplitude waves. This is marked with a green diamond. The green curve shows the maximal growth rate associated with this BF instability. At the secondary period-doubling bifurcation, $s_1^{1/2} = 0.128903$, marked with a green triangle, the first branch of the localized instability appears (maximal growth rate in black solid and dashed). The near-vertical appearance of this localized instability branch is a consequence of the rapid changes in the spectrum of this branch for steep waves. The inset $s \in [0.12878, 0.12908]$, $\gamma \in [0.005, 0.018]$ shows a zoom-in of the intersection of the maximal growth rate of the localized branch with the primary BF branch. The remnant of the BF instability merges with the localized branch at the edge of the gold region I. In this region, the BF branch is no longer distinguishable from the localized branch. The secondary branch of BF (maximal growth rate plotted in blue) emerges at the first maximizer of the speed at $s_{c,1} = 0.138753$ (blue diamond) and follows the same sequence of steps merging with the localized branch at the edge of the golden rectangle II. The secondary localized branch emerges at the second period-doubling bifurcation at $s_2^{1/2} = 0.140487$ (blue triangle). For the secondary inset $s \in [0.1404795, 0.1404955]$, $\gamma \in [0.005, 0.018]$. The tertiary BF emerges at the turning point of speed, $s_{c,2} = 0.140920$ (maximal growth rate plotted in purple), the tertiary localized branch appears at $s_3^{1/2} = 0.141032049$ (purple triangle).

3.6. *The high-frequency instabilities*

Since the work presented here focuses on the evolution of the spectrum for increasing steepness in the vicinity of the origin in the spectral plane, we discuss the high-frequency instabilities only briefly. As shown by Deconinck & Oliveras (2011) and Creedon *et al.* (2022), the high-frequency instabilities emanate from purely imaginary double eigenvalues for steepness $s = 0$, giving rise to an isola of unstable eigenvalues centred on the imaginary axis, away from the origin. As steepness is increased, these isole may collapse back on the imaginary axis, and new ones may form, see MacKay & Saffman (1986). Unlike the Benjamin–Feir (figure-8s) and localized instability branches (figure-∞s), the high-frequency isole are highly localized in the space of Floquet exponents: indeed, Deconinck & Oliveras (2011) show that often a range of Floquet exponents of width no more than 10^{-4} parameterizes an isola. This complicates their numerical detection. Figure 13 presents plots of a few high-frequency isole for near-extreme increasing steepness, showing the collapse of one into the imaginary axis. For the top isola plotted, $\mu \in [0.00092, 0.00095]$, for the one below $\mu \in [0.00057, 0.00059]$. For the two isole on bottom, $\mu \in [0.000251, 0.000294]$ (outer), $\mu \in [0.000263, 0.000282]$ (inner). This demonstrates the isole can be captured using our method. A detailed study of the evolution of the high-frequency instabilities as steepness increases is kept for future work.

4. Conclusions

We have presented a numerical exploration of the stability spectrum of Stokes waves near the origin of the spectral plane, focusing on the topological changes in the stability

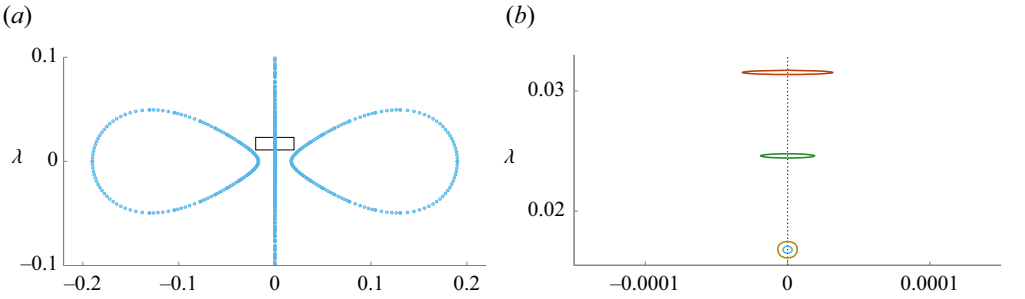

Figure 13. (*a*) Detached figure-∞ spectrum of the localized instability for $s = 0.1366171604 > s_{H,1}$ (blue). (*b*) Zoom-in on the high-frequency instability for four increasing values of the steepness, $s = 0.1366066477$ (red), $s = 0.1366141405$ (green), $s = 0.1366171424$ (golden) and $s = 0.1366171604$ (blue, the value (*a*)), showing the vanishing of a high-frequency isola at a value just exceeding $s = s_{H,1}$.

spectrum as the wave steepness grows. The main challenge of the study is due to the non-smooth nature of the extreme Stokes wave, which has a 120° corner at its crest. Thus, for waves whose steepness approaches that of this extreme wave, our Fourier-based method requires the use of millions of Fourier modes. Indeed, for the computation of waves with steepness near the third extremizer of the Hamiltonian (see figure 2) nearly 10^7 Fourier modes are used. To examine the stability of these waves, we linearize about them, resulting in a generalized operator eigenvalue problem. The numerical approximation of this problem results in a generalized matrix eigenvalue problem with matrices of dimension equal to the square of twice the number of Fourier modes used for approximating the underlying Stokes wave, since each component of the perturbation requires a comparable number of Fourier modes to reach the same accuracy. Storing and manipulating such matrices is prohibitive, and our investigations are only possible because of the matrix-free approaches to the conformal mapping formulation, introduced by Dyachenko & Semenova (2023*a*).

In Deconinck *et al.* (2023) we used this same method to investigate the largest growth rate of perturbations of near-extreme Stokes waves, as a function of their steepness. Among other outcomes, this led to the conclusion that long-lived ocean swell is confined to moderate amplitudes. In this paper, we focus instead on the behaviour of the stability spectrum near the origin of the spectral plane, as the recurring, self-similar behaviour may provide an indication of how the stability of near-extreme Stokes waves may be approached analytically. Specifically, previous work and our numerical explorations lead to the following conjectures.

(i) The Hamiltonian $\mathcal{H}$ and the velocity c have an infinite number of local extrema ($s_{H,n}$, $n = 1, 2, \ldots$ and $s_{c,n}$, $n = 0, 1, \ldots$, respectively) as the steepness s increases to s_{lim}, the steepness of the extreme wave. This conjecture is not new, and the asymptotics of Longuet-Higgins & Fox (1977, 1978) provide a strong indication as to its validity. We include this conjecture here because all others below depend upon it.

(ii) The maximal instability growth rate approaches infinity as the steepness increases to that of the steepest wave. Convincing evidence for this conjecture is presented by Korotkevich *et al.* (2023). This would imply that the Euler water wave problem for the evolution of the extreme Stokes wave is ill posed. This is not a surprise as capillary effects need to be incorporated when the curvature at the crest is too large. This is discussed in more detail by Deconinck *et al.* (2023).

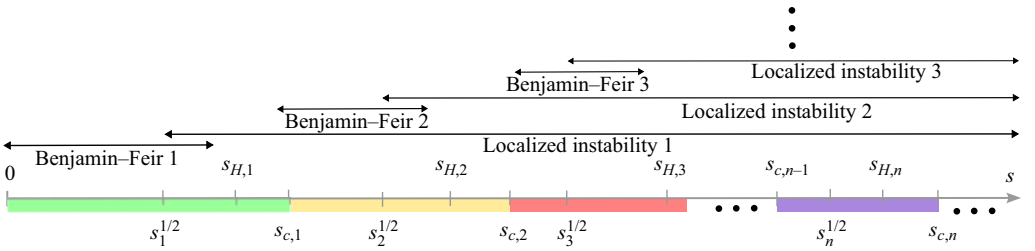

Figure 14. A schematic view of the appearance (and existence for a range of steepnesses) of localized and Benjamin–Feir type instabilities. The first Benjamin–Feir instability figure-8 appears at the steepness $s = s_{c,0} = 0$, the second one appears at $s = s_{c,1}$, and the third one at $s = s_{c,2}$. Localized instabilities, manifested by an oval at the origin deforming to a figure-∞ appear at steepnesses labelled $s_n^{1/2}$ with $n = 1, 2, 3, \ldots$, which correspond to bifurcations to double-period Stokes waves. Once localized instabilities appear, they continue to exist for all larger values of the steepness in contrast to Benjamin–Feir type instabilities that emerge and vanish as the steepness is increased. We conjecture that infinitely many Benjamin–Feir type and localized instabilities appear as $s \to s_{lim}$, the steepness of the extreme wave.

The conjectures below are a direct outcome of the investigations presented in this paper. A graphical overview of which features occur at which steepness, according to these conjectures, is presented in figure 14.

(iii) As the steepness s increases from 0 to that of the steepest wave, there exists an infinite number of Benjamin–Feir figure-8 instabilities. These emanate from the origin at each extremum $s_{c,n}$, $n = 0, 1, \ldots$ of the velocity. Upon formation, these figure-8s persist for a range of steepness. After their tangents at the origin become vertical (resulting in an hourglass shape) at steepness $s_{h,n}$, $n = 1, 2, \ldots$, the figure-8 separates in two lobes on the imaginary axis.

(iv) After the Benjamin–Feir figure-8 separates from the origin, the nth oval appears at the origin, for the steepness $s_n^{1/2}$, $n = 1, 2, \ldots$, corresponding to the period-doubling bifurcation points from the primary branch of Stokes waves.

(v) As the steepness s increases from 0 to that of the extreme wave, there are an infinite number of figure-∞ instabilities. These occur at the origin at each extremum of the Hamiltonian/energy. As the steepness is increased, the figure-∞s detach instantaneously. In other words, the figure-∞ shapes occur only at isolated values of the steepness, for which the Hamiltonian has a local extremum.

(vi) These figure-8s and figure-∞s alternate in their occurrence. Stated differently, the extremizers of the Hamiltonian interlace the extremizers of the velocity.

(vii) For Stokes waves with amplitude greater than that of the first maximizer of the Hamiltonian, the most unstable mode is either superharmonic (coperiodic) or subharmonic with twice the period of the Stokes wave (antiperiodic). Further, there exists an infinite number of interchanges between which of these two modes is dominant. Throughout these interchanges, no other mode is the most unstable. These observations were already discussed by Deconinck *et al.* (2023).

In the context of the full water wave problem, the present work reveals two primary mechanisms for the breaking of ocean waves: (i) for Stokes waves with $s < s_2 = 0.12894$ (the steepness at which the dominant instability switches from Benjamin–Feir to the localized branch, the abscissa of the green circle in figure 12), when the unstable envelope of multiple periods of a train of Stokes waves enters the nonlinear stage, a complicated pattern of waves is observed on the free surface. The pattern tends to self-focus leading to

the formation of a large unsteady wave whose crest forms a plunging breaker (Clamond *et al.* 2006; Onorato *et al.* 2013); (ii) for Stokes waves with $s > s_2$, the dynamics of the wave is dominated by the localized instability at the wave crest, see Dyachenko & Newell (2016), Baker & Xie (2011) and Duncan (2001). The localized instability immediately leads to wave breaking of either every other wave crest in the train (if $\mu = 0$ is dominant), or every other crest (if $\mu = 1/2$ is dominant) as discussed by Deconinck *et al.* (2023). More work is needed to understand the fully nonlinear stage of the many different instabilities computed.

A complete understanding of the stability of Stokes waves with respect to bounded perturbations (see Haragus & Kapitula 2008; Kapitula & Promislow 2013) requires further study of the spectrum of the operators associated with the linearization of the Euler equations governing the dynamics of these perturbed waves. Nonetheless, our study provides numerical evidence that the (quasi)periodic eigenfunctions that we examine, are fundamental to this problem.

Acknowledgements. The authors wish to thank E. Byrnes, D.M. Henderson and P.M. Lushnikov for helpful discussions. Also, the authors thank Frigo & Johnson (2005), the developers of FFTW and the whole GNU project for developing and supporting this important and free software. S.D. thanks the Isaac Newton Institute for Mathematical Sciences, Cambridge, UK, for support and hospitality during the programme 'Dispersive hydrodynamics' where work on this paper was partially undertaken. Partial support for A.S. is provided by a PIMS-Simons postdoctoral fellowship.

Declaration of interests. The authors report no conflict of interest.

Author ORCIDs.
S.A. Dyachenko https://orcid.org/0000-0003-1265-4055;
A. Semenova https://orcid.org/0000-0002-1303-1434.

References

Amick, C.J., Fraenkel, L.E. & Toland, J.F. 1982 On the Stokes conjecture for the wave of extreme form. *Acta Mathematica* **148** (1), 193–214.

Babenko, K.I. 1987 Some remarks on the theory of surface waves of finite amplitude. In *Doklady Akademii Nauk*, vol. 294, pp. 1033–1037. Russian Academy of Sciences.

Baker, G.R. & Xie, C. 2011 Singularities in the complex physical plane for deep water waves. *J. Fluid Mech.* **685**, 83–116.

Benjamin, T.B. 1967 Instability of periodic wavetrains in nonlinear dispersive systems. *Proc. R. Soc. Lond.* A **299** (1456), 59–76.

Benjamin, T.B. & Feir, J.E. 1967 The disintegration of wave trains on deep water. *J. Fluid Mech.* **27** (3), 417–430.

Berti, M., Maspero, A. & Ventura, P. 2022 Full description of Benjamin-Feir instability of Stokes waves in deep water. *Invent. Math.* **230** (2), 651–711.

Berti, M., Maspero, A. & Ventura, P. 2024 Stokes waves at the critical depth are modulationally unstable. *Commun. Math. Phys.* **405** (3), 56.

Bridges, T. & Mielke, A. 1995 A proof of the Benjamin-Feir instability. *Arch. Rat. Mech. Anal.* **133**, 145–198.

Chen, B. & Saffman, P.G. 1980 Numerical evidence for the existence of new types of gravity waves of permanent form on deep water. *Stud. Appl. Maths* **62** (1), 1–21.

Clamond, D., Francius, M., Grue, J. & Kharif, C. 2006 Long time interaction of envelope solitons and freak wave formations. *Eur. J. Mech.* B/*Fluids* **25** (5), 536–553.

Cowley, S.J., Baker, G.R. & Tanveer, S. 1999 On the formation of Moore curvature singularities in vortex sheets. *J. Fluid Mech.* **378**, 233–267.

Craig, W. & Sulem, C. 1993 Numerical simulation of gravity waves. *J. Comput. Phys.* **108**, 73–83.

Creedon, R. & Deconinck, B. 2023 A high-order asymptotic analysis of the Benjamin–Feir instability spectrum in arbitrary depth. *J. Fluid Mech.* **956**, A29.

Creedon, R.P., Deconinck, B. & Trichtchenko, O. 2022 High-frequency instabilities of Stokes waves. *J. Fluid Mech.* **937**, A24.

DECONINCK, B., DYACHENKO, S.A., LUSHNIKOV, P.M. & SEMENOVA, A. 2023 The dominant instability of near-extreme Stokes waves. *Proc. Natl Acad. Sci. USA* **120** (32), e2308935120.

DECONINCK, B. & KUTZ, J.N. 2006 Computing spectra of linear operators using the Floquet–Fourier–Hill method. *J. Comput. Phys.* **219** (1), 296–321.

DECONINCK, B. & OLIVERAS, K. 2011 The instability of periodic surface gravity waves. *J. Fluid Mech.* **675**, 141–167.

DUNCAN, J.H. 2001 Spilling breakers. *Annu. Rev. Fluid Mech.* **33**, 519–547.

DYACHENKO, A.I. 2001 On the dynamics of an ideal fluid with a free surface. In *Doklady Mathematics*, vol. 63, pp. 115–117. Pleiades Publishing.

DYACHENKO, A.I., KUZNETSOV, E.A., SPECTOR, M.D. & ZAKHAROV, V.E. 1996 Analytical description of the free surface dynamics of an ideal fluid (canonical formalism and conformal mapping). *Phys. Lett.* A **221** (1–2), 73–79.

DYACHENKO, S. & NEWELL, A.C. 2016 Whitecapping. *Stud. Appl. Maths* **137** (2), 199–213.

DYACHENKO, S.A., HUR, V.M. & SILANTYEV, D.A. 2023 Almost extreme waves. *J. Fluid Mech.* **955**, A17.

DYACHENKO, S.A., LUSHNIKOV, P.M. & KOROTKEVICH, A.O. 2014 The complex singularity of a Stokes wave. *JETP Lett.* **98** (11), 675–679.

DYACHENKO, S.A., LUSHNIKOV, P.M. & KOROTKEVICH, A.O. 2016 Branch cuts of Stokes wave on deep water. Part 1. Numerical solution and Padé approximation. *Stud. Appl. Maths* **137** (4), 419–472.

DYACHENKO, S.A. & SEMENOVA, A. 2023*a* Canonical conformal variables based method for stability of Stokes waves. *Stud. Appl. Maths* **150** (3), 705–715.

DYACHENKO, S.A. & SEMENOVA, A. 2023*b* Quasiperiodic perturbations of Stokes waves: secondary bifurcations and stability. *J. Comput. Phys.* **492**, 112411.

FRIGO, M. & JOHNSON, S.G. 2005 The design and implementation of FFTW3. *Proc. IEEE* **93** (2), 216–231.

GRANT, M.A. 1973 The singularity at the crest of a finite amplitude progressive Stokes wave. *J. Fluid Mech.* **59** (Part 2), 257–262.

HARAGUS, M. & KAPITULA, T. 2008 On the spectra of periodic waves for infinite-dimensional Hamiltonian systems. *Physica* D **237** (20), 2649–2671.

HAZIOT, S., HUR, V.M., STRAUSS, W.A., TOLAND, J.F., WAHLÉN, E., WALSH, S. & WHEELER, M.H. 2022 Traveling water waves – the ebb and flow of two centuries. *Q. Appl. Maths* **80**, 317–401.

HUR, V.M. 2006 Global bifurcation theory of deep-water waves with vorticity. *SIAM J. Math. Anal.* **37** (5), 1482–1521.

HUR, V.M. & YANG, Z. 2023 Unstable Stokes waves. *Arch. Rat. Mech. Anal.* **247** (4), 62.

KAPITULA, T. & PROMISLOW, K. 2013 *Spectral and Dynamical Stability of Nonlinear Waves*, Applied Mathematical Sciences, vol. 185. Springer.

KOROTKEVICH, A.O., LUSHNIKOV, P.M., SEMENOVA, A. & DYACHENKO, S.A. 2023 Superharmonic instability of Stokes waves. *Stud. Appl. Maths* **150** (1), 119–134.

LEVI-CIVITA, T. 1925 Détermination rigoureuse des ondes permanentes d'ampleur finie. *Math. Ann.* **93** (1), 264–314.

LIGHTHILL, M.J. 1965 Contributions to the theory of waves in non-linear dispersive systems. *IMA J. Appl. Maths* **1** (3), 269–306.

LONGUET-HIGGINS, M.S. 1975 Integral properties of periodic gravity waves of finite amplitude. *Proc. R. Soc. Lond.* A **342** (1629), 157–174.

LONGUET-HIGGINS, M.S. 1985 Bifurcation in gravity waves. *J. Fluid Mech.* **151**, 457–475.

LONGUET-HIGGINS, M.S. 2008 On an approximation to the limiting Stokes wave in deep water. *Wave Motion* **45** (6), 770–775.

LONGUET-HIGGINS, M.S. & FOX, M.J.H. 1977 Theory of the almost-highest wave: the inner solution. *J. Fluid Mech.* **80** (4), 721–741.

LONGUET-HIGGINS, M.S. & FOX, M.J.H. 1978 Theory of the almost–highest wave. Part 2. Matching and analytic extension. *J. Fluid Mech.* **85**, 769–786.

LONGUET-HIGGINS, M.S. & TANAKA, M. 1997 On the crest instabilities of steep surface waves. *J. Fluid Mech.* **336**, 51–68.

LUSHNIKOV, P.M. 2016 Structure and location of branch point singularities for Stokes waves on deep water. *J. Fluid Mech.* **800**, 557–594.

LUSHNIKOV, P.M., DYACHENKO, S.A. & SILANTYEV, D.A. 2017 New conformal mapping for adaptive resolving of the complex singularities of Stokes wave. *Proc. R. Soc.* A **473** (2202), 20170198.

MACKAY, R.S. & SAFFMAN, P.G. 1986 Stability of water waves. *Proc. R. Soc. Lond.* A **406** (1830), 115–125.

MAKLAKOV, D.V. 2002 Almost-highest gravity waves on water of finite depth. *Eur. J. Appl. Maths* **13** (1), 67.

MICHELL, J.H. 1893 XLIV. The highest waves in water. *Lond. Edinb. Dubl. Phil. Mag. J. Sci.* **36** (222), 430–437.

NEKRASOV, A.I. 1921 On waves of permanent type I. *Izv. Ivanovo-Voznesensk. Polite. Inst.* **3**, 52–65.
NGUYEN, H.Q. & STRAUSS, W.A. 2023 Proof of modulational instability of Stokes waves in deep water. *Commun. Pure Appl. Maths* **76** (5), 1035–1084.
ONORATO, M., RESIDORI, S., BORTOLOZZO, U., MONTINA, A. & ARECCHI, F.T. 2013 Rogue waves and their generating mechanisms in different physical contexts. *Phys. Rep.* **528** (2), 47–89.
OVSYANNIKOV, L.V. 1973 Dynamika sploshnoi sredy. Lavrentiev institute of hydrodynamics. *Sib. Branch Acad. Sci. USSR* **15**, 104.
PLOTNIKOV, P.I. 1982 Justification of the Stokes conjecture in the theory of surface waves (in Russian). *Dinamika Sploshnoi Sredy* **57**, 4176.
PLOTNIKOV, P.I. 2002 A proof of the Stokes conjecture in the theory of surface waves. *Stud. Appl. Maths* **108** (2), 217–244.
SAFFMAN, P.G. 1985 The superharmonic instability of finite-amplitude water waves. *J. Fluid Mech.* **159**, 169–174.
SCHWARTZ, L.W. 1974 Computer extension and analytic continuation of Stokes' expansion for gravity waves. *J. Fluid Mech.* **62** (3), 553–578.
SILANTYEV, D.A. 2019 A new conformal map for computing Stokes wave. Private communications.
STEWART, G.W. 2002 A Krylov-Schur algorithm for large eigenproblems. *SIAM J. Matrix Anal. Applics.* **23** (3), 601–614.
STOKES, G.G. 1847 On the theory of oscillatory waves. *Trans. Camb. Phil. Soc.* **8**, 441.
STOKES, G.G. 1880*a* On the theory of oscillatory waves. *Math. Phys. Papers* **1**, 197.
STOKES, G.G. 1880*b* Supplement to a paper on the theory of oscillatory waves. *Math. Phys. Papers* **1**, 314.
TANAKA, M. 1983 The stability of steep gravity waves. *J. Phys. Soc. Japan* **52** (9), 3047–3055.
TANAKA, M. 1985 The stability of steep gravity waves. Part 2. *J. Fluid Mech.* **156**, 281–289.
TANVEER, S. 1991 Singularities in water waves and Rayleigh–Taylor instability. *Proc. R. Soc. Lond.* A **435** (1893), 137–158.
TANVEER, S. 1993 Singularities in the classical Rayleigh–Taylor flow: formation and subsequent motion. *Proc. R. Soc. Lond.* A **441** (1913), 501–525.
TOLAND, J.F. 1978 On the existence of a wave of greatest height and Stokes's conjecture. *Proc. R. Soc. Lond.* A **363** (1715), 469–485.
TOLAND, J.F. 1996 Stokes waves. *Topol. Meth. Nonlinear Anal.* **7** (1), 1–48.
WHITHAM, G.B. 1967 Non-linear dispersion of water waves. *J. Fluid Mech.* **27** (2), 399–412.
WILLIAMS, J.M. 1981 Limiting gravity waves in water of finite depth. *Phil. Trans. R. Soc. Lond.* A **302** (1466), 139–188.
WILLIAMS, J.M. 1985 *Tables of Progressive Gravity Waves*. Pitman Advanced Pub. Program.
ZAKHAROV, V.E. 1968 Stability of periodic waves of finite amplitude on a surface. *J. Appl. Mech. Tech. Phys.* **9** (2), 190–194.
ZAKHAROV, V.E., KUZNETSOV, E.A. & DYACHENKO, A.I. 1996 Dynamics of free surface of an ideal fluid without gravity and surface tension. *Fizika Plasmy* **22**, 916–928.
ZUFIRIA, J.A. 1987 Non-symmetric gravity waves on water of infinite depth. *J. Fluid Mech.* **181**, 17–39.